JACS
JOURNAL OF THE AMERICAN CHEMICAL SOCIETY
Article
pubs.acs.org/JACS

Rational Design of an Efficient, Genetically Encodable, Protein-Encased Singlet Oxygen Photosensitizer

Michael Westberg,[†] Lotte Holmegaard,[†] Frederico M. Pimenta,[†] Michael Etzerodt,[‡] and Peter R. Ogilby*[,†]

[†]Center for Oxygen Microscopy and Imaging, Chemistry Department and [‡]Department of Molecular Biology and Genetics, Aarhus University, DK-8000, Aarhus, Denmark

Supporting Information

ABSTRACT: Singlet oxygen, $O_2(a^1\Delta_g)$, plays a key role in many processes of cell signaling. Limitations in mechanistic studies of such processes are generally associated with the difficulty of controlling the amount and location of $O_2(a^1\Delta_g)$ production in or on a cell. As such, there is great need for a system that (a) selectively produces $O_2(a^1\Delta_g)$ in appreciable and accurately quantifiable yields and (b) can be localized in a specific place at the suborganelle level. A genetically encodable, protein-encased photosensitizer is one way to achieve this goal. Through a systematic and rational approach involving mutations to a LOV2 protein that binds the chromophore flavin mononucleotide (FMN), we have developed a promising photosensitizer that overcomes many of the problems that affect related systems currently in use. Specifically, by decreasing the extent of hydrogen bonding between FMN and a specific amino acid residue in the local protein environment, we decrease the susceptibility of FMN to undesired photoinitiated electron-transfer reactions that kinetically compete with $O_2(a^1\Delta_g)$ production. As a consequence, our protein-encased FMN system produces $O_2(a^1\Delta_g)$ with the uniquely large quantum efficiency of 0.25 ± 0.03. We have also quantified other key photophysical parameters that characterize this sensitizer system, including unprecedented H_2O/D_2O solvent isotope effects on the $O_2(a^1\Delta_g)$ formation kinetics and yields. As such, our results facilitate future systematic developments in this field.

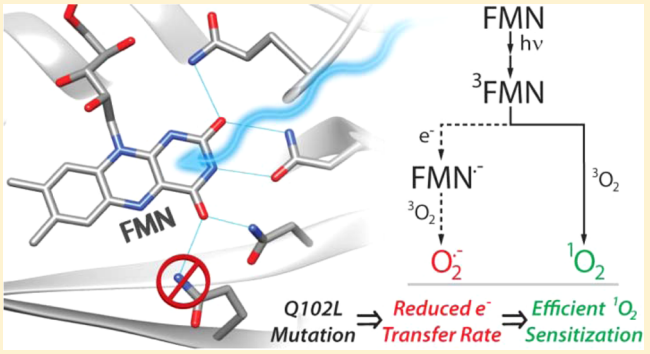

INTRODUCTION

Singlet oxygen, $O_2(a^1\Delta_g)$, the lowest energy excited electronic state of molecular oxygen, has a unique chemistry that can result in the oxidation and/or oxygenation of many organic and biologically relevant molecules.[1,2] Consequently, $O_2(a^1\Delta_g)$ is known to be an important intermediate in biological processes that range from cell death (apoptosis and necrosis) to cell proliferation (stimulated mitosis).[3−6] Although mechanistic studies designed to elucidate the behavior and action of $O_2(a^1\Delta_g)$ in cells have been performed for over ∼40 years, there is still much to be learned about the roles played by $O_2(a^1\Delta_g)$ in the spatially- and temporally-dependent processes of cell signaling.[4] A major limitation in this regard is associated with the difficulty of controlling and quantifying the amount and location of $O_2(a^1\Delta_g)$ production in or on a cell. Because $O_2(a^1\Delta_g)$ is conveniently produced via photosensitization,[3,7] one challenge of finding a solution to this problem depends, to a large extent, on developing a photosensitizer that allows for the controlled production of $O_2(a^1\Delta_g)$ in living cells. The development of such a sensitizer complements the equally important process of developing fluorescent probes for $O_2(a^1\Delta_g)$ that can likewise be localized in living cells.[8−10]

Over the years, attempts have been made to identify genetically encodable, protein-encased $O_2(a^1\Delta_g)$ sensitizers that could result in the photoinitiated perturbation of a cell.[3,11−16] Advantages of this approach include the fact that (a) protein tags facilitate controlled subcellular localization of the chromophore and (b) protein enclosures contribute to a controlled local environment for the chromophore that is ideally independent of its placement in or on a cell. However, to our knowledge, all of the systems developed thus far make $O_2(a^1\Delta_g)$ in very small yields (i.e., $O_2(a^1\Delta_g)$ quantum yield, ϕ_Δ, ≤0.09)[16] and/or principally function by producing reactive oxygen species (ROS) other than $O_2(a^1\Delta_g)$.[17] The ROS of particular relevance in this regard is the superoxide ion which is readily formed by photoinitiated electron-transfer reactions involving the sensitizer. The latter kinetically compete with the process of electronic energy transfer from the photoexcited sensitizer to ground-state oxygen, $O_2(X^3\Sigma_g^-)$, that results in the production of $O_2(a^1\Delta_g)$.

Of the genetically encodable protein-encapsulated sensitizers produced thus far, those using flavin mononucleotide (FMN) as the active chromophore have a great deal of potential for further development. A particularly relevant system produced by Shu et al.[14] was derived from *Arabidopsis thaliana* phototropin 2, exploiting the LOV2 flavin-binding domain of this protein. This system was called "miniSOG" for mini singlet

Received: November 21, 2014
Published: January 9, 2015

DOI: 10.1021/ja511940j
J. Am. Chem. Soc. 2015, 137, 1632−1642

oxygen generator.[14] It has recently been shown, however, that even though FMN efficiently produces $O_2(a^1\Delta_g)$ when dissolved in an aqueous solution (i.e., $\phi_\Delta(D_2O) = 0.65 \pm 0.04$),[18] the protein-encapsulated FMN in miniSOG only produces $O_2(a^1\Delta_g)$ in low yield ($\phi_\Delta = 0.03 \pm 0.01$).[18,19] Although different interpretations have been proposed for this observation,[19] we have shown that the low yield is a consequence of electron transfer from the protein to the FMN triplet state to produce the FMN radical anion, $FMN^{\bullet-}$.[18] This electron-transfer reaction effectively competes with the diffusion-dependent quenching of the ^{3}FMN state by $O_2(X^3\Sigma_g^-)$ to yield $O_2(a^1\Delta_g)$ (Scheme 1).[18] Subsequent

Scheme 1. Illustration of the Photoinitiated Processes in FMN Central to the Present Study[a]

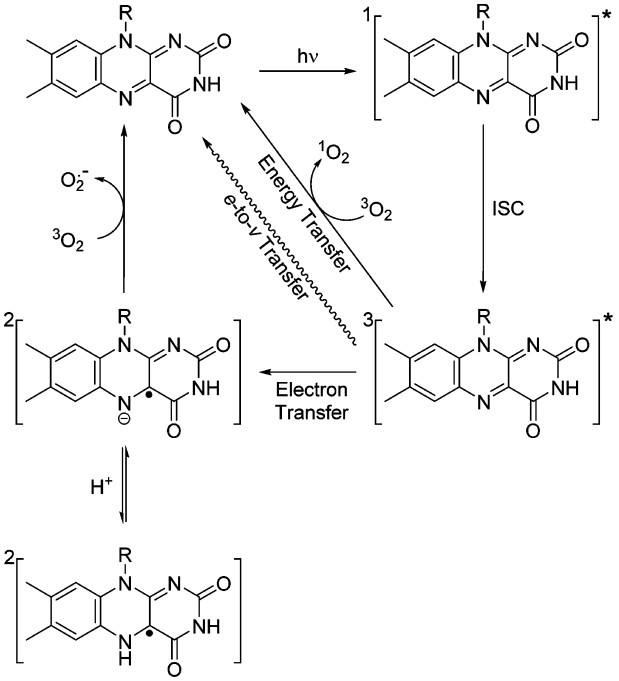

[a]Deactivation of the FMN triplet state by energy transfer to oxygen kinetically competes with (a) protein-mediated electron-transfer reactions and (b) nonradiative electronic-to-vibrational (*e*-to-*v*) energy dissipation. R refers to the ribityl-5′-phosphate "tail" in FMN.

diffusion-dependent quenching of the FMN radical anion by $O_2(X^3\Sigma_g^-)$ results in the formation of the superoxide ion via a second electron-transfer reaction that regenerates the neutral ground state of FMN (Scheme 1).[18] These photoinitiated electron-transfer reactions involving FMN have appreciable precedence in a wide range of studies,[20−22] including many that involve wild-type and mutated LOV proteins.[23−26]

If one is to retain basic features of the miniSOG system for the design of an efficient genetically encodable $O_2(a^1\Delta_g)$ photosensitizer (i.e., FMN in a LOV2-derived domain), it is clear that photoinduced protein-dependent electron-transfer reactions involving FMN must be suppressed in order to increase the probability of the competing energy-transfer process that results in $O_2(a^1\Delta_g)$ production. Because the miniSOG protein contains an "inactive" glycine residue[14] instead of the "active" electron-donating cysteine residue found in wild-type LOV proteins, the relevant electron donors to FMN must be amino acids at other positions in the miniSOG protein scaffold.[23,24,26]

For the rational redesign of the FMN-binding LOV2-based protein scaffold, with the goal of yielding a more efficient protein-encased $O_2(a^1\Delta_g)$ sensitizer, we found inspiration in studies illustrating the sensitivity of FMN photophysics and photoinduced electron-transfer reactions to its local hydrogen-bonding environment.[27−30] Our working hypothesis was based on the fact that the participation of FMN lone-pair electrons in a hydrogen bond with an adjacent amino acid residue decreases the net electron density on FMN.[27,31] Thus, such a hydrogen bond should make FMN more susceptible to photoreduction to form the radical anion. We therefore set out to perform systematic site-directed mutagenesis of residues in the miniSOG scaffold to decrease the extent of H-bonding to FMN without adversely affecting FMN binding in the protein. As outlined in the present report, one particular mutation in which a glutamine is replaced by a leucine (Q102L) has a positive effect on the $O_2(a^1\Delta_g)$ yield, yielding a reasonably efficient "singlet oxygen photosensitizing protein" (SOPP).

EXPERIMENTAL SECTION

Chemicals. The $O_2(a^1\Delta_g)$ photosensitizer phenalen-1-one-2-sulfonic acid (PNS) was synthesized as described in the literature.[32] The sources and purities of other chemicals and the description of buffer solutions used are provided in the Supporting Information.

Protein Mutation and Purification. Site-directed mutagenesis of the plasmid *p*miniSOG-BAD[33] encoding the miniSOG fusion protein was performed using a QuikChange Lightning Site-Directed Mutagenesis kit (Agilent Technologies) and oligonucleotide primers (Sigma-Aldrich) for mutagenesis and PCR amplification. Plasmids were transformed into competent *E. coli* XL1-Blue cells (Agilent Technologies), plasmid DNA isolated using the Nucleospin Plasmid kit (Machery-Nagel), and mutant sequences analyzed at GATC Biotech, Constance, Germany. Plasmids encoding the mutant fusion proteins were transformed into competent *E. coli* BL21 AI cells (Invitrogen). Protein expression was induced in growing cultures by addition of arabinose to 0.2% w/v following standard protocols. Cell growth and protein expression were always performed in the dark. The harvested cells were lysed by sonication in the purification buffer. Insoluble material was removed by centrifugation, and the soluble protein extract was batch adsorbed onto Ni-NTA agarose resin (Qiagen and Analytik Jena, respectively) and loaded onto an empty liquid chromatography glass column wrapped in aluminum foil. The protein loaded Ni-NTA column was washed with more than 10 column volumes of purification buffer. Bound fusion protein was eluted with the EDTA-containing buffer. The fusion proteins (yellow) eluted after the blue Ni-EDTA fraction. Fractions containing the fusion proteins were sampled in dark plastic tubes, and the purity of the proteins was analyzed by SDS-PAGE. Fractions were then buffer exchanged on PD-10 desalting columns (GE Healthcare) into PBS buffered D_2O or H_2O. Buffer changed fractions of the fusion protein were stored long-term at −80 °C or −20 °C and short-term at 4 °C in black tubes.

Further details are provided in the Supporting Information.

Instrumentation and Methods. All optical experiments were performed in 1 cm cuvettes at ∼23 °C.

Time-resolved $O_2(a^1\Delta_g) \rightarrow O_2(X^3\Sigma_g^-)$ phosphorescence measurements were performed using an approach and instrumentation that has previously been described.[34,35] For the present experiments, the protein-bound FMN was irradiated at 418 nm (fs laser, 1 kHz repetition rate, < 1.7 mW average power). The 1275 nm $O_2(a^1\Delta_g)$ phosphorescence signal was isolated using the combination of a cold mirror and a 1290 nm band-pass filter (fwhm 80 nm) and monitored using a cooled near-IR PMT operated in a photon counting mode. The sample absorbance at the irradiation wavelength of 418 nm did not exceed ∼0.1. Data were obtained over an elapsed period of sample irradiation where the absorbed energy did not exceed 14 J/mM for the proteins in D_2O solutions and 33 J/mM for the proteins in H_2O

DOI: 10.1021/ja511940j
J. Am. Chem. Soc. 2015, 137, 1632−1642

solutions. Under these conditions, where the sample volume was 3 mL, no irradiation-dependent changes in the ground-state absorption spectra and in the $O_2(a^1\Delta_g)$ kinetics were observed.

$O_2(a^1\Delta_g)$ experiments sensitized by Al(III) phthalocyanine chloride tetrasulfonic acid, $AlPcS_4$, were performed using 675 nm irradiation (fs output of an Optical Parametric Amplifier, Spectra Physics OPA-800C).

Transient absorption data were recorded with a "front-face" irradiation geometry where the fs laser pump beam was overlapped with the output of a *cw* 75 W Xe lamp (Oriel, model 66477) used as the probe beam. The fs laser, described previously,[34,35] was operated at a repetition rate of 67 Hz, and frequency-doubled pulses centered at 418 nm were used for these experiments. The laser beam was collimated to a diameter of ~3 mm yielding an irradiance of ~80 mW/cm^2. The output of the Xe lamp was passed through a water filter (Oriel, model 61945) and a 495 nm long pass filter. The probe beam was kept smaller than the pump beam throughout the propagation through the cuvette to avoid overlap associated distortion of the data.[36] The probe beam was coupled into a spectrograph (Andor Technology, Shamrock 303i) via an achromatic cylindrical lens (Thorlabs, ACY254−050-A). The detectors attached to the separate ports of the spectrograph were an iCCD camera (Andor Technology, iStar 320T-73) and a PMT (Hamamatsu model R928). The iCCD camera was used to record time-gated transient absorption spectra, averaged using 1000 laser shots at each time point with a temporal resolution of 50−100 ns. The PMT was used to record time-resolved traces. These traces were the average of 2000−5000 laser shots. In total, the absorbed energy was always <17 J/mM, a condition that yielded no observable irradiation-dependent changes in the kinetics of triplet-state decay and only minimal changes in the ground-state absorption spectra. The sample absorbance at the irradiation wavelength of 418 nm was 0.4−0.8 and the sample volume was 3 mL.

Steady-state absorption spectra were recorded on a Shimadzu model UV3600 UV−vis-NIR spectrometer and fluorescence spectra were recorded using a Fluoromax P spectrofluorometer (Horiba Jobin Yvon). Fluorescence quantum yield measurements were obtained using this spectrofluorometer under conditions where the sample absorbance did not exceed 0.05.

The hydroethidine, HE, experiments were performed using the spectrofluorometer for both sensitizer excitation at 440 nm and detection of fluorescence from the HE oxidation product. The latter experiments were performed with excitation at 525 nm and emission spectra recorded over the range 550−800 nm. Fresh stock solutions of HE in MeOH were always prepared and immediately added in equal amounts to the miniSOG and SOPP solutions to yield H_2O- or D_2O-based phosphate buffer containing 1% (v/v %) methanol. Data were recorded for solutions with initially identical miniSOG and SOPP absorbance at 440 nm. Solutions were constantly stirred during the experiments.

miniSOG Illustration. The miniSOG structure shown in Figure 1 was obtained by sequence homology alignment using SWISS MODEL[37] with a template sequence identity of 96.19% corresponding to a crystal structure[38] of a mutant of the LOV2 domain of *Arabidopsis thaliana* phototropin 2 (PDB ID: 4EET).

RESULTS AND DISCUSSION

Site-Directed Mutagenesis: General Overview. Site-directed mutagenesis was employed to generate a variety of systems in which the local environment of the protein-bound FMN differed from that found in miniSOG. Two general directions were explored. First, we focused on the residue at position 39. In wild-type LOV2 proteins, this position is occupied by a cysteine that participates in the formation of a photoadduct with FMN.[39] In the preparation of miniSOG, this cysteine was replaced by a glycine.[14] For the present study, we examined mutants in which this glycine residue was replaced by a number of other amino acids (e.g., G39S) to examine the possible effect of a change in the electrostatic potential around

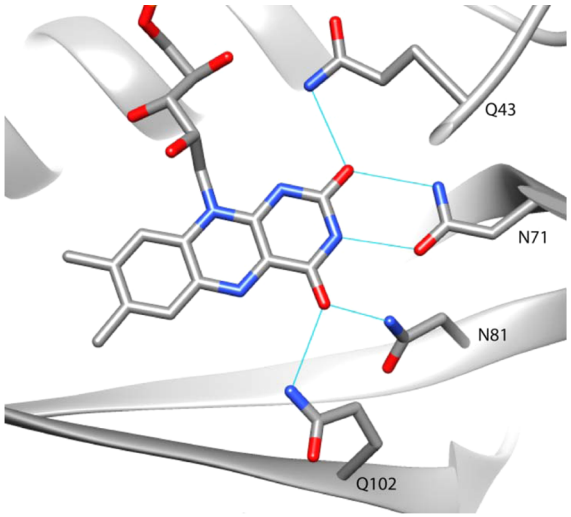

Figure 1. Illustration that shows the four conserved residues with hydrogen bonds to FMN in miniSOG. With the exception of one H-bond involving N71, all of the H-bonds shown result in an effective decrease in the electron density on FMN.[31]

FMN. Second, and most importantly, we examined mutants that involved changes in the four conserved residues that form hydrogen bonds with FMN in miniSOG (Figure 1).[38−40]

Of the mutations examined, several lead to a decrease in FMN binding (see Supporting Information). This was observed as a loss of yellow color during the expression and purification process. This is arguably not surprising given that the binding of FMN in LOV proteins is sensitive to mutations in the binding pocket.[41−43] However, four mutations (i.e., G39A, G39P, G39S, and Q102L) yielded proteins that were easily purified without loss of FMN.

A preliminary screening of selected photophysical properties of these four mutants, in particular a determination of ϕ_Δ in D_2O, indicated that G39A, G39P, and G39S did not differ much from what was observed with miniSOG itself (see Supporting Information). In contrast, the Q102L mutant in which a glutamine residue that H-bonds to FMN is replaced by a non-H-bonding leucine produced $O_2(a^1\Delta_g)$ in a much higher yield than that observed with miniSOG. On this basis, and for ease in our remaining discussion, we refer to this new Q102L mutant as "SOPP".

To establish a solid framework to better elucidate the factors that result in the apparent differences in these ϕ_Δ values, we set out to investigate in greater detail selected photophysical properties of SOPP, miniSOG, and FMN.

Absorption and Fluorescence Spectra. Absorption and fluorescence spectra of SOPP, miniSOG, and FMN were recorded in H_2O- and D_2O-based phosphate buffer solutions (pH 7.4 and pD 7.8, respectively). When performing $O_2(a^1\Delta_g)$ experiments, it is often advantageous to record data in a deuterated solvent to exploit the large H/D solvent isotope effect on the $O_2(a^1\Delta_g)$ lifetime ($\tau_\Delta(D) \gg \tau_\Delta(H)$).[3,7] The spectra thus obtained for each of these three molecules were the same in both H_2O- and D_2O-based solutions (Figure 2).

The protein-dependent appearance of structure on the FMN spectra is consistent with what has previously been observed and is attributed to vibronic transitions in the more structurally confined molecule.[14,18,44,45] Although SOPP and miniSOG show similar vibronic structure, the SOPP spectra are systematically blue-shifted relative to the miniSOG spectra

DOI: 10.1021/ja511940j
J. Am. Chem. Soc. 2015, 137, 1632−1642

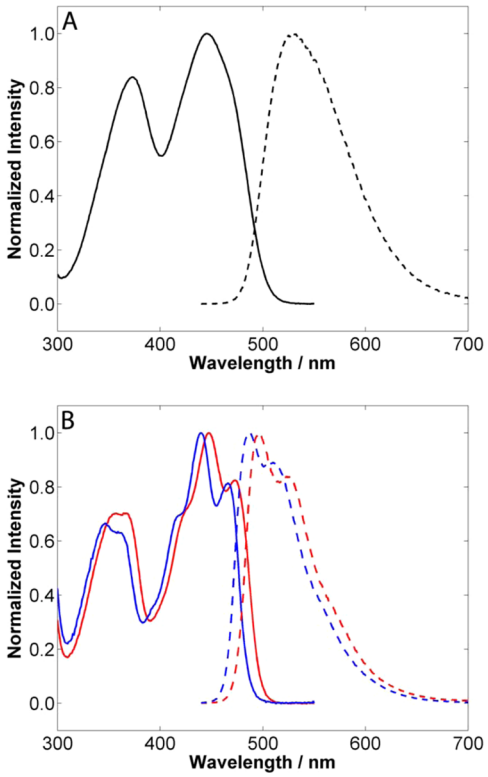

Figure 2. (A) Normalized absorption (solid line) and fluorescence (dashed line) spectra of FMN. (B) Normalized absorption (solid lines) and fluorescence (dashed lines) spectra of miniSOG (red) and SOPP (blue).

(Figure 2B). Thus, relative to miniSOG, the Q102L mutation either stabilizes the FMN ground state or destabilizes the FMN Franck–Condon and geometrically relaxed singlet excited states, or both. These data are consistent with what has been observed from related mutations in other LOV proteins.[46−48]

Molar extinction coefficients at the absorption band maxima, ε_{max}, were determined for the flavoproteins in H_2O-based phosphate buffer solutions using a technique whereby the bound FMN was released from the protein scaffold via alkaline denaturation (see Supporting Information). Within our margins of error, we observe that SOPP and miniSOG have the same extinction coefficient at the absorption band maximum (Table 1). Moreover, our results agree with what has been published on FMN in LOV proteins in general.[46]

Fluorescence quantum yields, ϕ_f, were determined in both H_2O and D_2O (Table 1). Within our error margins, miniSOG and SOPP have similar fluorescence yields. Moreover, encasing FMN in the proteins causes a slight increase in the fluorescence yield, reflecting our use of the FMN and miniSOG data from Wingen et al.[46] as our ϕ_f standards. The data also indicate that there is no H/D solvent isotope effect on ϕ_f. This observation is pertinent in light of data presented below.

Production of the FMN Radical Anion and Neutral Semiquinone. A key aspect of our earlier study on miniSOG was the observation of the characteristic absorption spectrum[28,49,50] of the protonated FMN radical anion (i.e., neutral semiquinone) upon irradiation of miniSOG in a deoxygenated aqueous solution.[18] As outlined in the Introduction and shown in Scheme 1, this species arises as a consequence of photoinitiated electron transfer from the protein matrix to FMN. In the current study, we were likewise able to record this characteristic spectrum upon irradiation of deoxygenated solutions of miniSOG at 418 nm (Figure 3A). Moreover, we could record this spectrum long after irradiation of miniSOG ceased, confirming that this semiquinone is reasonably stable in

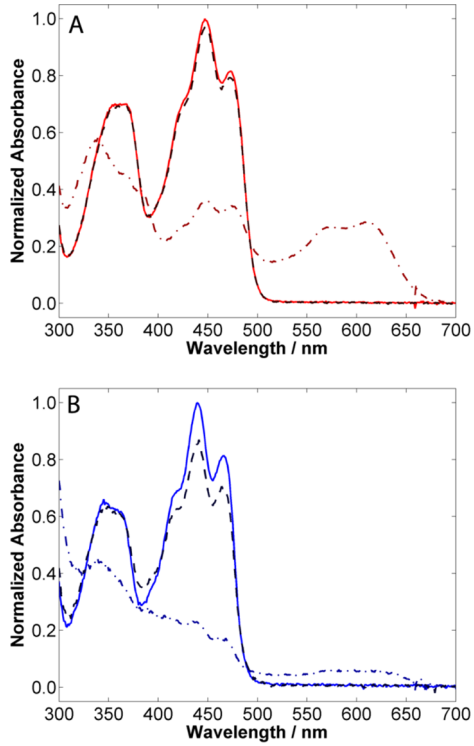

Figure 3. Absorption spectra of miniSOG (A) and SOPP (B) in H_2O-based phosphate buffer solution before irradiation (solid lines), after 15 min irradiation of a deoxygenated solution (dashed-dotted line), and after air-equilibration in the dark (dashed line).

Table 1. Absorption and Emission Properties of FMN, miniSOG, and SOPP[a]

	$\lambda_{abs,\ max}$ (nm)	ε_{max} ($mM^{-1}\ cm^{-1}$)	$\lambda_{emission,\ max}$ (nm)	ϕ_f	
	H_2O/D_2O	H_2O	H_2O/D_2O	H_2O	D_2O
FMN	445 ± 1	12.3 ± 0.1	531 ± 1	0.25 ± 0.01[b]	0.25 ± 0.02
miniSOG	447 ± 1	14.1 ± 0.3	496 ± 1	0.41 ± 0.01[b]	0.45 ± 0.06
SOPP	440 ± 1	14.5 ± 0.5	487 ± 1	0.45 ± 0.06	0.43 ± 0.06

[a]Recorded from air-saturated solutions. All solutions were buffered (pH 7.4, pD 7.8). [b]Data from Wingen et al.[46] We used the ϕ_f value reported for FMN in H_2O-based buffer as the standard for our D_2O FMN experiment. The ϕ_f value reported for miniSOG in H_2O-based buffer was used as the standard for all our flavoprotein experiments. The data of Wingen et al. were recorded using an integrating sphere and, thus, are presumably not susceptible to polarization effects. We did not use an integrating sphere or polarizers in our experiments. Thus, our experimental approach to quantify ϕ_f does not account for possible changes in the fluorescence anisotropy in the flavoprotein solutions.

DOI: 10.1021/ja511940j
J. Am. Chem. Soc. 2015, 137, 1632−1642

the absence of oxygen. Upon exposing our irradiated solution of miniSOG to the oxygen-containing ambient atmosphere, the spectrum of the semiquinone disappeared, and we almost completely recovered the original spectrum of miniSOG (Figure 3A). These observations are consistent with the deprotonation and oxidation of the FMN semiquinone back to neutral FMN by $O_2(X^3\Sigma_g^-)$ to yield the superoxide ion. Irradiation of SOPP under the same deoxygenated conditions likewise yields a band characteristic of the FMN semiquinone (Figure 3B). The relative intensity of this band appears smaller than that observed upon irradiation of miniSOG, and as such, this could be one indication that the Q102L mutation indeed has the desired effect, i.e., we have been able to decrease the susceptibility of ^{3}FMN to one-electron reduction by the protein. However, we are hesitant to rest on this interpretation based solely on these particular data since it appears that other irradiation-induced changes may be concurrently occurring in SOPP under these conditions. For example, we do not completely recover the original SOPP spectrum upon exposure of the irradiated solution to the ambient atmosphere (Figure 3B). In this regard, it is important to note that, under the present conditions, we did not observe an increase in the absorbance of the SOPP sample over the range ~300−375 nm. The latter is characteristic of tryptophan oxidation in the protein.[18,51,52] We return to this point in a separate section below.

Time-Resolved Transient Absorption Spectra. *Assigning Spectra to ^{3}FMN.* Transient absorption spectra were recorded over the range 525−850 nm from FMN, miniSOG, and SOPP upon fs pulsed laser irradiation of these compounds at 418 nm in H_2O- and D_2O-based phosphate buffer solutions (Figures 4 and S3). Experiments were performed in air-saturated solutions in order to (a) preclude potentially complicating self-quenching reactions that are observed for free FMN under deaerated conditions,[20,21,30] (b) avoid complications associated with the accumulation of the protein-encased FMN semiquinone that are likewise observed under deaerated conditions (see Figure 3), and (c) best complement the kinetic conditions under which $O_2(a^1\Delta_g)$ is formed in these systems. Spectra were recorded using a gated iCCD camera under conditions in which the first spectrum was recorded 200 ns after the irradiating pulse (e.g., data shown in Figure 4A), and thereafter at periodic intervals extending out to 1 ms after the irradiating pulse (e.g., data shown in Figure 4B). Other than an overall decrease in intensity, the spectra recorded at these later times did not differ appreciably from that recorded at 200 ns after the irradiating pulse (Figure 4B). Thus, the transient spectrum over the period of 1 ms after the irradiating pulse appears to be dominated by one species. Indeed, upon monitoring the decrease in signal intensity at different wavelengths over the range 525−850 nm, the data could be fitted with a single exponential decay function. The latter was confirmed in independent transient absorption experiments performed at 725 nm using a PMT as the detector that allowed for the collection of significantly more data points over the time course of the signal decay (Figures 4B and S3). For FMN dissolved in the H_2O-based buffer solution, the lifetime thus obtained was 3.2 ± 0.2 μs in air-saturated solutions and 0.65 ± 0.05 μs in oxygen-saturated solutions (Table 2). If we assume an $O_2(X^3\Sigma_g^-)$ concentration of 0.27 mM under our aerated conditions and 1.27 mM under our oxygenated conditions,[53,54] these data yield a rate constant for the quenching of this transient species by $O_2(X^3\Sigma_g^-)$ of 1.2 × 10^9 s^{-1} M^{-1}, a number which is consistent for the quenching of a triplet excited state in a liquid solvent.[54] Indeed, the spectra obtained are consistent with what has previously been reported for the triplet states of riboflavin[22,50] and FMN in a LOV protein.[26,55] Thus, we assign the spectra shown in Figure 4 to the FMN triplet state. This assignment is consistent with the recent report showing that, in a LOV2 protein, the neutral FMN semiquinone is not formed in appreciable yields in aerated solutions and that the anionic semiquinone absorbs very weakly over the spectral range 525−850 nm (see Scheme 1).[26,28,49]

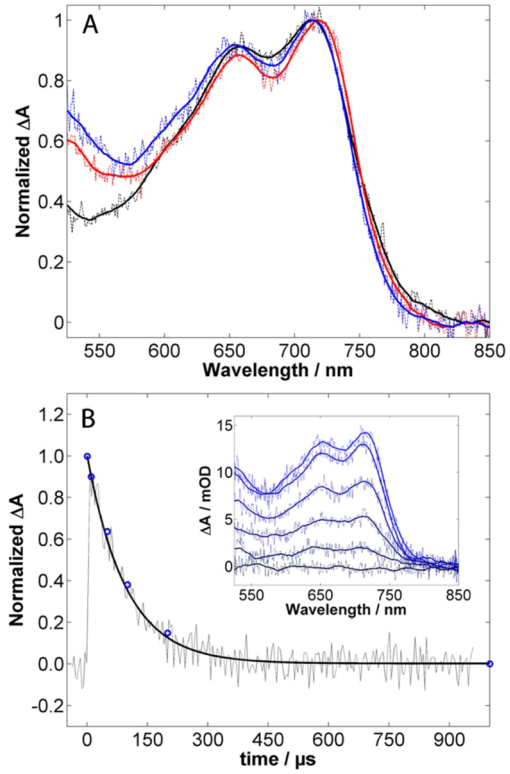

Figure 4. (A) Transient absorption spectra of FMN (black), miniSOG (red), and SOPP (blue) in aerated buffered H_2O. The results of a smoothing operation (solid lines) have been applied to the raw data (broken lines). (B) Time-resolved absorption trace of SOPP in H_2O at 725 nm independently recorded using a PMT (gray) and the associated single exponential fit (black line). The corresponding data recorded with the gated iCCD camera (integrated transient absorption between 650 and 750 nm recorded at six time points; blue open circles) agrees with the higher resolution PMT trace. (insert) Transient absorption over the range 525−850 nm at 0.2, 10, 20, 100, 200, and 1000 μs after the irradiating pulse, respectively.

The Mechanistic Core Reflected in Protein Effects on τ_T. We observed a significant increase in the lifetime of this triplet state, τ_T, going from solvated FMN to miniSOG to SOPP (Table 2). We can interpret these data in terms of three kinetically competing processes that define the core of our overall problem. First, enclosing FMN in the protein results in a decrease in the rate constant for quenching of ^{3}FMN by $O_2(X^3\Sigma_g^-)$ (i.e., the protein shields FMN, providing a more tortuous path through which $O_2(X^3\Sigma_g^-)$ must diffuse). For example, the SOPP data in Table 2 yield an effective rate constant for ^{3}FMN quenching by $O_2(X^3\Sigma_g^-)$ of ~1.1 × 10^7 s^{-1} M^{-1} which is indeed appreciably smaller than the value of 1.2 × 10^9 s^{-1} M^{-1} recorded for solvated FMN (*vide supra*). Second, the observation that τ_T(SOPP) > τ_T(miniSOG) could reflect

DOI: 10.1021/ja511940j
J. Am. Chem. Soc. 2015, 137, 1632−1642

Table 2. Photophysical Properties of FMN, miniSOG, and SOPP[a]

	τ_T (μs)		relative ϕ_T[b]		ϕ_Δ	
	H_2O	D_2O	H_2O	D_2O	H_2O	D_2O
FMN	3.2 ± 0.2[c]	3.2 ± 0.2[c]	0.89	1.0	0.49 ± 0.05	0.65 ± 0.05
	0.65 ± 0.05 (O_2)	0.66 ± 0.05 (O_2)				
miniSOG	31 ± 3	39 ± 4	0.95	0.99	0.05 ± 0.02	0.04 ± 0.01
SOPP	100 ± 10	130 ± 10	1.0	0.99	0.19 ± 0.03	0.25 ± 0.03
	48 ± 5 (O_2)[d]					

[a]Recorded from air-saturated solutions unless otherwise noted. All solutions were buffered (pH 7.4, pD 7.8). [b]The relative triplet quantum yields, ϕ_T, of miniSOG and SOPP are comparable and have been normalized to the quantum yield of SOPP in H_2O. The corresponding triplet yields for FMN should not be compared to those for miniSOG and SOPP (see text). Errors on these numbers are ~±10% of the value shown. [c]Data were independent of the FMN concentration over the range 45−90 μM, indicating that FMN-dependent self-quenching reactions that are seen under deaerated conditions[20,21,30] do not compete with the quenching of ^{3}FMN by oxygen under our conditions. [d]Obtained from the $O_2(a^1\Delta_g)$ phosphorescence signal (see text), not from a direct triplet absorption experiment.

the desired result that the Q102L mutation indeed mitigates electron transfer from the protein to ^{3}FMN. Third, the Q102L mutation could change the rate of nonradiative ^{3}FMN deactivation. We return to these points in separate sections below. In any event, the longer ^{3}FMN lifetime in SOPP certainly correlates with the higher SOPP-sensitized $O_2(a^1\Delta_g)$ yield compared to miniSOG (e.g., ϕ_Δ (SOPP, D_2O) = 0.25 ± 0.03, whereas ϕ_Δ (miniSOG, D_2O) = 0.04 ± 0.01). As mentioned at the outset and as further discussed in a separate section below, this difference in $O_2(a^1\Delta_g)$ quantum yields is a key aspect of our report and demonstrates that our approach is indeed successful.

H_2O/D_2O Effects on τ_T. Continuing with our discussion of the FMN triplet-state lifetimes, it is clear that, for both miniSOG and SOPP, τ_T is longer in D_2O-based solutions than in H_2O-based solutions (Table 2). Recent data suggest that τ_T in a related LOV protein does not change over the pH range of 6.5−10.0.[26] Thus, our observations are not likely a result of the simple difference between pH 7.4 and pD 7.8. Rather, to interpret our observation, we first note that truncated LOV-domain proteins readily exchange backbone protons to deuterons when the solvent is changed from H_2O to D_2O.[56] It is also known that (a) the overall protein structure is largely unaffected by this H/D change[23] and (b) a change in the surrounding bulk solvent from H_2O to D_2O can result in a more stable and less flexible protein.[56−59] Nevertheless, certainly for SOPP, a putative isotope-dependent reduction in protein flexibility does not appear to reduce the rate of ^{3}FMN quenching by $O_2(X^3\Sigma_g^-)$ because we see a large value of ϕ_Δ in D_2O (Table 2).

It is more reasonable to conclude that the observed change in τ_T reflects the effect that H/D substitution has on the rate of nonradiative ^{3}FMN deactivation (see Scheme 1). Solvent H/D isotope effects on the deactivation rate of an excited-state solute have been examined for many years (i.e., solute-to-solvent electronic-to-vibrational, *e*-to-*v*, energy transfer). One pertinent example is the pronounced H/D solvent isotope effect on $O_2(a^1\Delta_g)$ nonradiative deactivation which, to a large extent, is a consequence of the fact that oxygen has only one vibrational degree of freedom and thus cannot efficiently dissipate the excitation energy of $O_2(a^1\Delta_g)$ (i.e., coupling to solvent vibrational modes in this case provides a more efficient energy sink).[7,60] For larger molecular solutes, in particular a sensitizer triplet state, the situation is more complicated. In the least, one must first consider that *e*-to-*v* energy-transfer kinetically competes with quenching by $O_2(X^3\Sigma_g^-)$ (i.e., in aerated and oxygenated solutions we do not observe a H_2O/D_2O effect on FMN τ_T; see Table 2). Upon minimizing the effects of quenching by $O_2(X^3\Sigma_g^-)$ through experiments performed under conditions of low $O_2(X^3\Sigma_g^-)$ concentration, and in cases where solute coupling to the solvent is strong, H → D substitution in the solvent can be manifested as an increase in the triplet lifetime.[61,62] For our present examples of miniSOG and SOPP, where the protein enclosure decreases the efficiency of ^{3}FMN quenching by $O_2(X^3\Sigma_g^-)$, our data suggest that FMN coupling to the protein matrix likewise becomes sufficiently important.

With the preceding model in mind, it remains to explain why τ_T would be longer in a D_2O-based medium than in a H_2O-based medium. The basis for one possible answer is found in established discussions of *e*-to-*v* energy transfer.[63] We first note that higher frequency vibrational modes (e.g., O−H bonds) are better energy sinks than lower frequency modes (e.g., O−D bonds).[7,60,62−65] Thus, the *e*-to-*v* process should become less efficient under the combined conditions of (a) proton to deuteron exchange in the protein and (b) strong coupling between FMN and the protein. Moreover, given that a change in the surrounding bulk solvent from H_2O to D_2O can result in a less flexible protein,[57−59] the corresponding decrease in the vibrational and rotational degrees of freedom of the total system could likewise result in a poorer sink for the electronic excitation energy of the protein-encased ^{3}FMN.

A different explanation for our observed H_2O/D_2O effects on τ_T does not directly involve *e*-to-*v* transfer but, rather, is related to the working hypothesis that forms the basis of the present study. Specifically, upon proton to deuteron exchange at selected places in the protein and in FMN, the nature of the hydrogen bond(s) between FMN and the residues Q43, N71, and/or N81 could change (i.e., bond distance, bond angle) such that the electron density at FMN could increase thereby reducing the susceptibility of ^{3}FMN to reduction.

Quantifying ϕ_T. Within the noise levels of our experiments, the triplet spectra obtained in D_2O-based solutions were the same as those obtained in H_2O-based solutions (Figures 4 and S3). If we assume that, over the range 525−850 nm, the wavelength-dependent molar extinction coefficient for ^{3}FMN in SOPP is the same as that for ^{3}FMN in miniSOG, then we can integrate the respective spectra to yield relative values for the quantum yield of ^{3}FMN formation, ϕ_T. (This same treatment cannot be extended to include solvated FMN because the transient absorption spectra and ground-state extinction coefficients are slightly different. Thus, in this case, we can only compare data recorded in H_2O with those recorded in D_2O.)

DOI: 10.1021/ja511940j
J. Am. Chem. Soc. 2015, 137, 1632−1642

The data thus obtained indicate that the Q102L mutation does not appreciably affect the yield of ^{3}FMN in these respective proteins (Table 2), which is consistent with published data on related systems.[29,30] This is also consistent with our observation that quantum yields of fluorescence are likewise independent of the surrounding protein (Table 1). All of this supports the model where electron transfer from the protein occurs to ^{3}FMN and not ^{1}FMN (Scheme 1). Furthermore, given that these triplet states are comparatively long-lived, the distance-dependent electron transfer to ^{3}FMN can occur from amino acid residues that are comparatively far away.[66,67] This latter point has ramifications that are addressed further in separate sections below.

$O_2(a^1\Delta_g)$ Phosphorescence Experiments. The direct, time-resolved detection of $O_2(a^1\Delta_g) \rightarrow O_2(X^3\Sigma_g^-)$ phosphorescence at ~1275 nm was used to investigate (a) the kinetics of $O_2(a^1\Delta_g)$ production and decay and (b) the efficiency of $O_2(a^1\Delta_g)$ formation in these sensitized experiments. All experiments were performed with freshly prepared protein solutions, low excitation intensities, and short irradiation periods because prolonged irradiation of these samples results in complicated changes in the $O_2(a^1\Delta_g)$ kinetics that are not easily characterized (*vide infra*).[18]

General Kinetics. Under ideal conditions, the formation of $O_2(a^1\Delta_g)$ in a triplet-state photosensitized process will follow first-order kinetics with a rate constant k_T that represents all processes for the deactivation of the triplet-state sensitizer (Figure 5).[3] However, even if the kinetics of $O_2(a^1\Delta_g)$ formation deviate from single exponential behavior, as often happens for sensitizers in nonhomogeneous environments, an independent time-resolved experiment to characterize the kinetics of the sensitizer's triplet-state decay yields data that can be used to characterize the time-resolved $O_2(a^1\Delta_g)$ signals.[3] As we have established (*vide supra*), triplet-state decay in both SOPP and miniSOG follows clean first-order kinetics under our conditions. Likewise, under ideal conditions, the sum of all processes that remove $O_2(a^1\Delta_g)$ can be represented using a first-order rate constant k_Δ (Figure 5). The latter is most accurately characterized by fitting time-resolved $O_2(a^1\Delta_g)$ phosphorescence signals with a function that includes the rate constant k_T for $O_2(a^1\Delta_g)$ formation that has been independently determined (Figure 5).

For the sensitized production of $O_2(a^1\Delta_g)$ under conditions in which the sensitizer is dissolved in a bulk solvent with ready access to quenching by $O_2(X^3\Sigma_g^-)$, the inequality $k_T \gg k_\Delta$ is generally observed, and values of k_Δ are easily obtained from time-resolved $O_2(a^1\Delta_g)$ phosphorescence data. A pertinent exception occurs when using H_2O as the solvent. In this case, the comparatively low concentration of dissolved $O_2(X^3\Sigma_g^-)$ and an efficient process of solvent-mediated $O_2(a^1\Delta_g)$ deactivation can combine to yield $k_T \sim k_\Delta$ or even $k_\Delta > k_T$. To increase the accuracy in analyzing such data, D_2O is often used as the solvent because $k_\Delta(D_2O) < k_\Delta(H_2O)$.[3,7] Similarly, under conditions in which the excited-state sensitizer is not readily accessible to quenching by $O_2(X^3\Sigma_g^-)$, $k_T \sim k_\Delta$, or $k_\Delta > k_T$. This latter situation is characteristic of many caged or encased sensitizers,[3,18,68] including the flavoproteins used in the present study. Nevertheless, the $O_2(a^1\Delta_g)$ data from such systems can still be accurately quantified as long as values of k_T can be independently determined and used in the fitting functions (Figure 5, Table 2 where $\tau_T = 1/k_T$).

SOPP- and miniSOG-Sensitized τ_Δ Values. In the absence of any quenching by a solute, τ_Δ in D_2O is ~67 μs.[60] Values of

$$^3M \xrightarrow[O_2(X^3\Sigma_g^-)]{k_{ET}} O_2(a^1\Delta_g) \xrightarrow{k_\Delta} \text{removal of } O_2(a^1\Delta_g)$$

$$\left[O_2(a^1\Delta_g)\right]_t = \frac{k_{ET}\left[O_2(X^3\Sigma_g^-)\right]\left[^3M\right]_0}{k_\Delta - k_T}\left(e^{-k_T t} - e^{-k_\Delta t}\right)$$

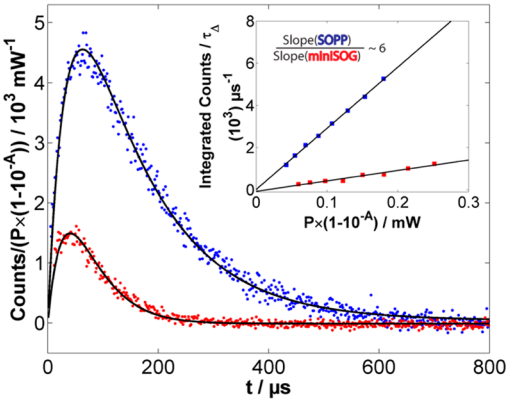

Figure 5. (top) General kinetic scheme for the sensitized production of $O_2(a^1\Delta_g)$ by the triplet state of a given molecule M. The rate constant k_{ET} quantifies the energy-transfer process, and k_Δ represents all channels for $O_2(a^1\Delta_g)$ removal. (middle) Equation based on this scheme that describes the evolution of $O_2(a^1\Delta_g)$ in time subsequent to pulsed laser excitation of M. $[^3M]_0$ is the triplet-state concentration at time = 0, and the first-order rate constant k_T represents all channels for ^3M removal, including those that do not result in $O_2(a^1\Delta_g)$ formation. (bottom) Representative time-resolved $O_2(a^1\Delta_g)$ phosphorescence data for the SOPP (blue) and miniSOG (red) sensitized production of $O_2(a^1\Delta_g)$ in a D_2O-based buffer solution. The black lines are fits to the data using the above-mentioned equation. (insert) Plots showing the numerical integral of the $O_2(a^1\Delta_g)$ signal, normalized by the $O_2(a^1\Delta_g)$ lifetime, against the power absorbed by the sample (i.e., the relative number of excited states produced). The slopes are proportional to the quantum yield of $O_2(a^1\Delta_g)$ production.

$\tau_\Delta = 1/k_\Delta$ obtained from fits to $O_2(a^1\Delta_g)$ phosphorescence data such as those shown in Figure 5 for SOPP- and miniSOG-sensitized experiments in D_2O-based buffer solutions (τ_Δ = 34 ± 3 μs and τ_Δ = 40 ± 4 μs, respectively) indicate that these flavoproteins also quench $O_2(a^1\Delta_g)$. To further elucidate these particular values of τ_Δ for these flavoprotein samples, we used $AlPcS_4$ to independently photosensitize the production of $O_2(a^1\Delta_g)$ in the bulk solvent surrounding SOPP and, independently, miniSOG. Specifically, under conditions in which the sample was not diluted, we added $AlPcS_4$ to the same sample from which a given flavoprotein-sensitized value of τ_Δ was obtained, and then the corresponding values of τ_Δ were determined upon irradiation of $AlPcS_4$. Within the errors of our measurement, the τ_Δ values thus obtained upon irradiation of $AlPcS_4$ were identical to the τ_Δ values obtained upon irradiation of SOPP and miniSOG, respectively (*vide supra*). The results of this τ_Δ experiment thus indicate that an appreciable amount of $O_2(a^1\Delta_g)$ produced by FMN in these flavoproteins is able to diffuse out of the enclosing protein and, over its lifetime, experience the same general environment as a $O_2(a^1\Delta_g)$ molecule produced in the bulk solvent by $AlPcS_4$.

In an earlier publication, Ruiz-González et al.[19] hypothesized that the low yield of miniSOG-sensitized $O_2(a^1\Delta_g)$ measured in a $O_2(a^1\Delta_g)$ phosphorescence experiment was a consequence of the quenching of a presumably large amount of nascent $O_2(a^1\Delta_g)$ by the enclosing protein. This presentation is not consistent with our present τ_Δ results, obtained using the

DOI: 10.1021/ja511940j
J. Am. Chem. Soc. 2015, 137, 1632−1642

simple kinetic scheme shown in Figure 5, combined with the other results in our present study (e.g., τ_T and ϕ_Δ). Indeed, there is a growing body of evidence to indicate that appreciable amounts of $O_2(a^1\Delta_g)$ can diffuse through some rather complicated protein environments.[3,10,69,70]

SOPP- and miniSOG-Sensitized ϕ_Δ Values. Values of τ_Δ obtained from our $O_2(a^1\Delta_g)$ data are important as a parameter used to normalize the integrated intensity of the $O_2(a^1\Delta_g)$ phosphorescence signal in the procedure[71] to obtain the quantum yield of sensitized $O_2(a^1\Delta_g)$ production, ϕ_Δ, for these respective flavoproteins. The pertinent experiments were performed using the phosphorescence intensity of $O_2(a^1\Delta_g)$ sensitized by PNS in D_2O or H_2O as a reference standard ($\phi_\Delta = 0.97 \pm 0.06$),[72] and the resultant data are shown in Table 2.

The miniSOG and FMN ϕ_Δ data obtained in the present study are consistent with what has been published.[18,19,73] Most importantly, the Q102L mutation to produce SOPP clearly has a positive effect on the $O_2(a^1\Delta_g)$ yield. Although the SOPP-sensitized yield of $O_2(a^1\Delta_g)$ is still not as large as that of FMN freely dissolved in an aqueous solution, it is appreciably larger than the miniSOG-sensitized yield of $O_2(a^1\Delta_g)$. This result thus adds credence to the validity of our approach to mitigate protein-mediated electron-transfer reactions to ^{3}FMN. The ϕ_Δ value of 0.25 ± 0.03 for SOPP is certainly large enough for use in mechanistic studies of $O_2(a^1\Delta_g)$.

The ϕ_Δ data in Table 2 also reveal an unexpected phenomenon which, to our knowledge, has no precedence: we find that the yields of both FMN- and SOPP-sensitized $O_2(a^1\Delta_g)$ are greater in D_2O than in H_2O. (Values of miniSOG-sensitized ϕ_Δ are too small to warrant a corresponding evaluation.) Although these results are surprising, they can nevertheless both be partially explained using the τ_T and ϕ_T data also reported in Table 2. Specifically, for SOPP, it is reasonable to correlate the $\phi_\Delta(D_2O) > \phi_\Delta(H_2O)$ inequality with the $\tau_T(D_2O) > \tau_T(H_2O)$ inequality, i.e., with a longer triplet lifetime, a larger fraction of the triplet states can be quenched by $O_2(X^3\Sigma_g^-)$ to yield $O_2(a^1\Delta_g)$. For FMN, the solvent isotope effect on ϕ_T likewise appears to be consistent with the corresponding ϕ_Δ values. Nevertheless, more experiments need to be done to properly interpret this observation.

Characterizing and Quantifying SOPP-Sensitized ROS other than $O_2(a^1\Delta_g)$. With comparatively small elapsed irradiation doses, the postulated principal photoinitiated process that characterizes the behavior of miniSOG is electron transfer from the protein to ^{3}FMN to produce the FMN radical anion which, in turn, transfers an electron to $O_2(X^3\Sigma_g^-)$ to produce the superoxide ion.[18] Evidence to support this perspective included experiments in which miniSOG photooxidized hydroethidine (HE) to yield a fluorescent product with an emission maximum at ~600−610 nm.[18] This transformation of HE provides a useful probe for a variety of ROS.[74] Most importantly, this transformation of HE does not occur upon interaction with $O_2(a^1\Delta_g)$.[18,75,76]

Although SOPP produces more $O_2(a^1\Delta_g)$ than miniSOG (i.e., $\phi_\Delta(SOPP)/\phi_\Delta(miniSOG) \sim 6$), this does not preclude the possibility that SOPP still produces an appreciable amount of the superoxide ion as a consequence of a photoinitiated electron-transfer reaction. In short, a SOPP $O_2(a^1\Delta_g)$ quantum yield of ~0.25 still leaves plenty of room for other photoinitiated processes to occur. With this in mind, we used correlated experiments to monitor the extent to which SOPP and miniSOG oxidized HE in D_2O solutions (Figure 6). The data obtained indicate that SOPP produces ~1.3 times more non-$O_2(a^1\Delta_g)$ ROS than miniSOG (i.e., $HE_{ox}(SOPP)/HE_{ox}(miniSOG) \sim 1.3$).

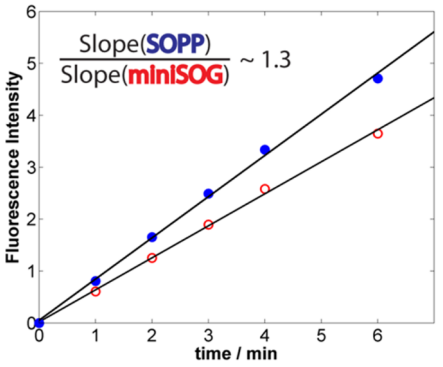

Figure 6. Fluorescence intensity from the HE oxidation product, integrated over the wavelength range 575−800 nm, formed by 440 nm irradiation of SOPP (filled circles) and miniSOG (open circles) plotted against the elapsed time of steady-state irradiation. The initial integrated background signal of each sample has been subtracted from all the data points. Data were recorded from miniSOG and SOPP samples with identical absorbance at 440 nm ($A = 0.080 \pm 0.003$) dissolved in the D_2O-based phosphate buffer with 1% (by volume) of added methanol. The solid lines are linear fits to the data and are consistent with the expectation that HE oxidation is a zero-order process at the limit of low [ROS]. Corresponding data recorded from H_2O solutions give the same result (Figure S6) indicating that radicals that might derive from $O_2(a^1\Delta_g)$-mediated photooxygenation of the protein do not contribute to these data.

It is important to interpret this result in the context of the kinetically competing processes that characterize our systems (Scheme 1) and that give rise to the data shown in Table 2. First, we must recognize that, in aerated solutions, FMN in SOPP has a much longer triplet-state lifetime than FMN in miniSOG (i.e., $k_T(SOPP) < k_T(miniSOG)$). This point, combined with the observations that $\phi_\Delta(SOPP)/\phi_\Delta(miniSOG) \sim 6$ and $HE_{ox}(SOPP)/HE_{ox}(miniSOG) \sim 1.3$, indicates that our working hypothesis is correct and that the Q102L mutation used to make SOPP indeed yields the desired effect of reducing the rate of electron transfer from the protein to FMN. However, in itself, the observation that $HE_{ox}(SOPP)/HE_{ox}(miniSOG) \sim 1.3$ indicates that the Q102L mutation must also influence k_T in ways other than just changing the rate of electron-transfer reactions involving ^{3}FMN. Specifically, if we assume that the overall rate of ^{3}FMN quenching by $O_2(X^3\Sigma_g^-)$ is the same in miniSOG and SOPP, our data combine to indicate that the rate constant for nonradiative ^{3}FMN deactivation in miniSOG must be greater than that in SOPP. Although our original working hypothesis regarding H-bonding between FMN and the conserved amino acid residues in the protein was cast in the context of altering the probability of electron-transfer reactions, this same hypothesis equally applies to the kinetically competing process of *e*-to-*v* transfer (*vide supra*). In short, the Q102L mutation could result in poor coupling of FMN to the protein matrix thereby causing a decrease in the component of nonradiative decay that contributes to k_T.

Effects of Prolonged Irradiation. Earlier studies of miniSOG-sensitized $O_2(a^1\Delta_g)$ production demonstrated that the yield of $O_2(a^1\Delta_g)$ increased appreciably upon prolonged irradiation of miniSOG.[18,19] In our studies on this point,[18] we found that this increase in the $O_2(a^1\Delta_g)$ yield, as measured

DOI: 10.1021/ja511940j
J. Am. Chem. Soc. 2015, 137, 1632−1642

through the integrated intensity of the $O_2(a^1\Delta_g)$ phosphorescence signal, was accompanied by an increase in the complexity of the kinetics of $O_2(a^1\Delta_g)$ formation and decay.

With this in mind, we set out to examine both miniSOG and SOPP under related conditions of prolonged irradiation at 418 nm, extending the total amount of accumulated absorbed energy to much larger values than those examined in our earlier study on miniSOG. These experiments were performed in aerated solutions of buffered D_2O. The data obtained are shown in Figure 7.

For both miniSOG and SOPP, we find appreciable bleaching of the principal chromophore as seen by the decrease in the absorption band centered at ~450 nm. Note that there appears to be only a decrease in band intensity; the relative positions of the vibronic transitions remain unchanged. This indicates that "undegraded" FMN remains bound by the protein throughout the process (also see Figure 2). This bleaching is accompanied by an increase in sample absorbance over the wavelength range ~300−350 nm that could represent the combination of products of both FMN and protein decomposition. It is important to note that these photoinduced changes occur faster in D_2O-based solutions than in H_2O-based solutions. Given the established D_2O/H_2O solvent isotope effect on the lifetime of $O_2(a^1\Delta_g)$,[7,60] this latter observation suggests that $O_2(a^1\Delta_g)$ is a reactive intermediate involved in these bleaching reactions.

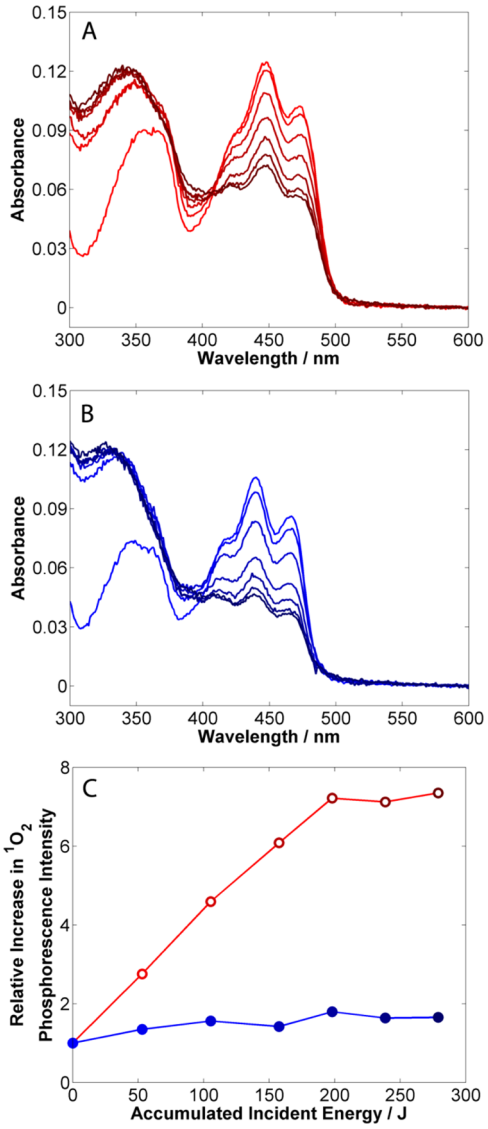

Figure 7. Effects of elapsed irradiation on the absorption spectra of miniSOG (A) and SOPP (B). (C) The correlated plots of miniSOG-sensitized (open circles) and SOPP-sensitized (filled circles) intensities of $O_2(a^1\Delta_g)$ phosphorescence as a function of the accumulated energy incident on the sample cuvettes. The data in each of these latter plots were normalized to the corresponding $O_2(a^1\Delta_g)$ intensity at small amounts of accumulated energy.

Coincident with this rather extensive irradiation-induced decomposition of the chromophores, we observe an increase in the integrated intensity of the $O_2(a^1\Delta_g)$ phosphorescence signals at 1275 nm (Figure 7C). Thus, photoinduced decomposition of both miniSOG and SOPP produces a better $O_2(a^1\Delta_g)$ sensitizer than the well-characterized parent systems. In the least, these data account for published reports in which miniSOG is used as, and claimed to be, an efficient $O_2(a^1\Delta_g)$ sensitizer.[14,77] However, the extent to which irradiation changes the miniSOG-sensitized $O_2(a^1\Delta_g)$ phosphorescence intensity is much greater than that observed with SOPP. Thus, one clear advantage of the SOPP system is that its propensity to produce $O_2(a^1\Delta_g)$ remains more constant upon prolonged irradiation.

This increase in the intensity of $O_2(a^1\Delta_g)$ phosphorescence with an increase in the elapsed time of irradiation is also accompanied by an increase in the complexity of the time-resolved $O_2(a^1\Delta_g)$ kinetic traces (see Supporting Information). Such data likely reflect a combination of different processes since amino acid residues in these flavoproteins (His, Met, Trp, and Tyr) can act as electron donors as well as $O_2(a^1\Delta_g)$ quenchers.[78,79] Thus, for example, the observed decrease in the rate of sensitized $O_2(a^1\Delta_g)$ formation upon prolonged irradiation, which correlates with a decrease in the rate of ^{3}FMN decay, likely reflects the oxidation, and hence removal, of amino acids that can quench ^{3}FMN by electron transfer. This interpretation is also consistent with the observed irradiation-dependent increase in the $O_2(a^1\Delta_g)$ phosphorescence intensity. The removal of electron-donating amino acid residues could likewise have a pronounced effect on the lifetime of $O_2(a^1\Delta_g)$ by decreasing the concentration of effective $O_2(a^1\Delta_g)$ quenchers. Finally, observed deviations from the simple exponential expression shown in Figure 5 suggest that, under our conditions, these processes of photooxidation yield an inhomogeneous distribution of degraded flavoproteins in our sample cuvette.

Does SOPP Provide the Desired Solution? Does SOPP solve the current need for an efficient genetically encodable $O_2(a^1\Delta_g)$ photosensitizer, or is it just a step in the correct direction? Given the data in this paper, the answers to these questions are reasonably straightforward.

First, if miniSOG can be used as a genetically encodable $O_2(a^1\Delta_g)$ photosensitizer for experiments in live cells,[80,81] even with all of its rather significant limitations, then SOPP most certainly provides a much better option in this regard. Second, SOPP definitely provides a prominent step in the correct direction in terms of the selectivity of the ROS produced. The evidence for this is that the Q102L mutation clearly decreases the rate of electron transfer from the protein to ^{3}FMN resulting in a comparatively long lifetime of ^{3}FMN in SOPP. As such, the quenching of ^{3}FMN by $O_2(X^3\Sigma_g^-)$ becomes more competitive, resulting in a higher yield of $O_2(a^1\Delta_g)$.

Nevertheless, there is still significant room for improvement with SOPP. First, note that the ^{3}FMN lifetimes of ~100 μs in SOPP were recorded using air-saturated solutions. The

DOI: 10.1021/ja511940j
J. Am. Chem. Soc. 2015, 137, 1632−1642

observation of such a relatively long lifetime under these conditions clearly indicates that $O_2(X^3\Sigma_g^-)$ does not efficiently diffuse through the protein enclosure; efficient quenching of ^{3}FMN by $O_2(X^3\Sigma_g^-)$ would reduce τ_T to approximately <5 μs. Although we have decreased the overall rate of the electron-transfer reaction from the protein to ^{3}FMN, electron transfer still effectively competes with the quenching of ^{3}FMN by $O_2(X^3\Sigma_g^-)$ as seen in the results of the HE assay (Figure 6). One solution to this problem involves a mutation of the protein that will provide $O_2(X^3\Sigma_g^-)$ better access to the chromophore without (a) adversely affecting the binding of FMN in the protein and (b) facilitating access to the chromophore of other larger solutes that could also quench ^{3}FMN and that might be added to the solution as mechanistic tools (e.g., NaN_3 to quench $O_2(a^1\Delta_g)$).

CONCLUSIONS

Through a rational approach, we have produced a genetically encodable protein-encased photosensitizer that makes $O_2(a^1\Delta_g)$ in appreciable yield. Working with FMN bound in a LOV2-derived protein, a mutant was produced that decreased the extent of hydrogen bonding to FMN and thereby decreased the susceptibility of FMN to undesired reactions that kinetically compete with $O_2(a^1\Delta_g)$ production. We have also determined key kinetic parameters that characterize this protein-encased chromophore system, thereby facilitating future systematic developments. The use of such protein-encased sensitizers that can be specifically localized in a living cell will be a great mechanistic asset in studies of $O_2(a^1\Delta_g)$-mediated signaling processes.

ASSOCIATED CONTENT

Supporting Information

Sources of selected chemicals and the description of buffer solutions used, additional procedural details on protein mutation, determination of flavoprotein extinction coefficients, transient absorption data in D_2O and H_2O solutions, time-resolved $O_2(a^1\Delta_g)$ phosphorescence data in H_2O solutions and upon prolonged irradiation of the flavoprotein, and hydro-ethidium experiments in H_2O solutions. This material is available free of charge via the Internet at http://pubs.acs.org.

AUTHOR INFORMATION

Corresponding Author

*progilby@chem.au.dk

Notes

The authors declare no competing financial interest.

ACKNOWLEDGMENTS

This work was supported by grants from the Danish National Research Foundation and the EU Marie Curie Training Program (TopBio PITN-GA-2010-264362). The authors thank Roger Y. Tsien (University of California-San Diego) for providing the miniSOG plasmid, Anette Kjems and Puk Lund (Aarhus University) for assistance with the expression and purification of the proteins, and Rasmus L. Jensen (Aarhus University) for helpful discussions.

REFERENCES

(1) Clennan, E. L.; Pace, A. *Tetrahedron* **2005**, *61*, 6665−6691.
(2) Davies, M. J. *Biochem. Biophys. Res. Commun.* **2003**, *305*, 761−770.
(3) Ogilby, P. R. *Chem. Soc. Rev.* **2010**, *39*, 3181−3209.
(4) Redmond, R. W.; Kochevar, I. E. *Photochem. Photobiol.* **2006**, *82*, 1178−1186.
(5) Klotz, L.-O.; Kröncke, K.-D.; Sies, H. *Photochem. Photobiol. Sci.* **2003**, *2*, 88−94.
(6) Blázquez-Castro, A.; Breitenbach, T.; Ogilby, P. R. *Photochem. Photobiol. Sci.* **2014**, *13*, 1235−1240.
(7) Schweitzer, C.; Schmidt, R. *Chem. Rev.* **2003**, *103*, 1685−1757.
(8) Kim, S.; Tachikawa, T.; Fujitsuka, M.; Majima, T. *J. Am. Chem. Soc.* **2014**, *136*, 11707−11715.
(9) Pedersen, S. K.; Holmehave, J.; Blaikie, F. H.; Gollmer, A.; Breitenbach, T.; Jensen, H. H.; Ogilby, P. R. *J. Org. Chem.* **2014**, *79*, 3079−3087.
(10) Pimenta, F. M.; Jensen, J. K.; Etzerodt, M.; Ogilby, P. R. *Photochem. Photobiol. Sci.* **2015**, DOI: 10.1039/c1034pp00408f.
(11) Bulina, M. E.; Chudakov, D. M.; Britanova, O. V.; Yanushevich, Y. G.; Staroverov, D. B.; Chepurnykh, T. V.; Merzlyak, E. M.; Shkrob, M. A.; Lukyanov, S.; Lukyanov, K. A. *Nat. Biotechnol.* **2006**, *24*, 95−99.
(12) Jimenez-Banzo, A.; Ragas, X.; Abbruzzetti, S.; Viappiani, C.; Campanini, B.; Flors, C.; Nonell, S. *Photochem. Photobiol. Sci.* **2010**, *9*, 1336−1341.
(13) Takemoto, K.; Matsuda, T.; Sakai, N.; Fu, D.; Noda, M.; Uchiyama, S.; Kotera, I.; Arai, Y.; Horiuchi, M.; Fukui, K.; Ayabe, T.; Inagaki, F.; Suzuki, H.; Nagai, T. *Sci. Rep.* **2013**, *3*, 2629.
(14) Shu, X.; Lev-Ram, V.; Deerinck, T. J.; Qi, Y.; Ramko, E. B.; Davidson, M. W.; Jin, Y.; Ellisman, M. H.; Tsien, R. Y. *PLoS Biology* **2011**, *9*, e1001041.
(15) Ragàs, X.; Cooper, L. P.; White, J. H.; Nonell, S.; Flors, C. *ChemPhysChem* **2011**, *12*, 161−165.
(16) Torra, J.; Burgos-Caminal, A.; Endres, S.; Wingen, M.; Drepper, T.; Gensch, T.; Ruiz-González, R.; Nonell, S. *Photochem. Photobiol. Sci.* **2015**, DOI: 10.1039/c4PP00338A.
(17) Vegh, R. B.; Solntsev, K. M.; Kuimova, M. K.; Cho, S.; Liang, Y.; Loo, B. L. W.; Tolbert, L. M.; Bommarius, A. S. *Chem. Commun.* **2011**, *47*, 4887−4889.
(18) Pimenta, F. M.; Jensen, R. L.; Breitenbach, T.; Etzerodt, M.; Ogilby, P. R. *Photochem. Photobiol.* **2013**, *89*, 1116−1126.
(19) Ruiz-González, R.; Cortajarena, A. L.; Mejias, S. H.; Agut, M.; Nonell, S.; Flors, C. *J. Am. Chem. Soc.* **2013**, *135*, 9564−9567.
(20) Görner, H. *J. Photochem. Photobiol. B: Biol.* **2007**, *87*, 73−80.
(21) Heelis, P. F. *Chem. Soc. Rev.* **1982**, *11*, 15−39.
(22) Lu, C.; Lin, W.; Wang, W.; Han, Z.; Yao, S.; Lin, N. *Phys. Chem. Chem. Phys.* **2000**, *2*, 329−334.
(23) Kay, C. W. M.; Schleicher, E.; Kuppig, A.; Hofner, H.; Rudiger, W.; Schleicher, M.; Fischer, M.; Bacher, A.; Weber, S.; Richter, G. *J. Biol. Chem.* **2003**, *278*, 10973−10982.
(24) Lanzl, K.; Sanden-Flohe, M.; Kutta, R.-J.; Dick, B. *Phys. Chem. Chem. Phys.* **2010**, *12*, 6594−6604.
(25) Eisenreich, W.; Fischer, M.; Romisch-Margl, W.; Joshi, M.; Richter, G.; Bacher, A.; Weber, S. *Biochem. Soc. Trans.* **2009**, *37*, 382−386.
(26) Kutta, R. J.; Magerl, K.; Kensy, U.; Dick, B. *Photochem. Photobiol. Sci.* **2015**, DOI: 10.1039/c4PP00155a.
(27) Yagi, K.; Ohishi, N.; Nishimoto, K.; Choi, J. D.; Song, P. S. *Biochemistry* **1980**, *19*, 1553−1557.
(28) Miura, R. *Chem. Rec.* **2001**, *1*, 183−194.
(29) Raffelberg, S.; Mansurova, M.; Gärtner, W.; Losi, A. *J. Am. Chem. Soc.* **2011**, *133*, 5346−5356.
(30) Valle, L.; Vieyra, F. E. M.; Borsarelli, C. D. *Photochem. Photobiol. Sci.* **2012**, *11*, 1051−1061.
(31) Nishimoto, K.; Fukumaga, H.; Yagi, K. *J. Biochem.* **1986**, *100*, 1647−1653.
(32) Nonell, S.; Gonzalez, M.; Trull, F. R. *Afinidad* **1993**, *448*, 445−450.
(33) Available at: http://www.tsienlab.ucsd.edu/Samples/Constructs.htm.
(34) Arnbjerg, J.; Johnsen, M.; Frederiksen, P. K.; Braslavsky, S. E.; Ogilby, P. R. *J. Phys. Chem. A* **2006**, *110*, 7375−7385.

DOI: 10.1021/ja511940j
J. Am. Chem. Soc. 2015, 137, 1632−1642

(35) Salice, P.; Arnbjerg, J.; Pedersen, B. W.; Toftegaard, R.; Beverina, L.; Pagani, G. A.; Ogilby, P. R. *J. Phys. Chem. A* **2010**, *114*, 2518−2525.
(36) Bazin, M.; Ebbesen, T. W. *Photochem. Photobiol.* **1983**, *37*, 675−678.
(37) Arnold, K.; Bordoli, L.; Kopp, J.; Schwede, T. *Bioinformatics* **2006**, *22*, 195−201.
(38) Christie, J. M.; Hitomi, K.; Arvai, A. S.; Hartfield, K. A.; Mettlen, M.; Pratt, A. J.; Tainer, J. A.; Getzoff, E. D. *J. Biol. Chem.* **2012**, *287*, 22295−22304.
(39) Losi, A.; Gärtner, W. *Photochem. Photobiol.* **2011**, *87*, 491−510.
(40) List, N. H.; Pimenta, F. M.; Holmegaard, L.; Jensen, R. L.; Etzerodt, M.; Schwabe, T.; Kongsted, J.; Ogilby, P. R.; Christiansen, O. *Phys. Chem. Chem. Phys.* **2014**, *16*, 9950−9959.
(41) Salomon, M.; Christie, J. M.; Knieb, E.; Lempert, U.; Briggs, W. R. *Biochemistry* **2000**, *39*, 9401−9410.
(42) Jones, M. A.; Feeney, K. A.; Kelly, S. M.; Christie, J. M. *J. Biol. Chem.* **2007**, *282*, 6405−6414.
(43) Zayner, J. P.; Antoniou, C.; French, A. R.; Hause, R. J.; Sosnick, T. R. *Biophys. J.* **2013**, *105*, 1027−1036.
(44) Schüttrigkeit, T. A.; Kompa, C. K.; Salomon, M.; Rüdiger, W.; Michel-Beyerle, M. E. *Chem. Phys.* **2003**, *294*, 501−508.
(45) Klaumünzer, B.; Kröner, D.; Saalfrank, P. *J. Phys. Chem. B* **2010**, *114*, 10826−10834.
(46) Wingen, M.; Potzkei, J.; Endres, S.; Casini, G.; Rupprecht, C.; Fahlke, C.; Krauss, U.; Jaeger, K.-E.; Drepper, T.; Gensch, T. *Photochem. Photobiol. Sci.* **2014**, *13*, 875−883.
(47) Nash, A. I.; Ko, W.-H.; Harper, S. M.; Gardner, K. H. *Biochemistry* **2008**, *47*, 13842−13849.
(48) Nozaki, D.; Iwata, T.; Ishikawa, T.; Todo, T.; Tokutomi, S.; Kandori, H. *Biochemistry* **2004**, *43*, 8373−8379.
(49) Massey, V. *Biochem. Soc. Trans.* **2000**, *28*, 283−296.
(50) Li, H.; Melø, T. B.; Naqvi, K. R. *J. Photochem. Photobiol., B* **2012**, *106*, 34−39.
(51) Walrant, P.; Santus, R. *Photochem. Photobiol.* **1974**, *19*, 411−417.
(52) Fukunaga, Y.; Katsuragi, Y.; Izumi, T.; Sakiyama, F. *J. Biochem.* **1982**, *92*, 129−141.
(53) *IUPAC Solubility Data Series*; Battino, R., Ed.; Pergamon Press: Oxford, 1981; Vol. 7: Oxygen and Ozone.
(54) Montalti, M.; Credi, A.; Prodi, L.; Gandolfi, M. T. *Handbook of Photochemistry*; 3rd ed.; CRC Press: Boca Raton, 2006.
(55) Bauer, C.; Rabi, C.-R.; Heberle, J.; Kottke, T. *Photochem. Photobiol.* **2011**, *87*, 548−553.
(56) Lee, C.-T.; Malzahn, E.; Brunner, M.; Mayer, M. P. *J. Mol. Biol.* **2014**, *426*, 601−610.
(57) Cioni, P.; Strambini, G. B. *Biophys. J.* **2002**, *82*, 3246−3253.
(58) Parker, M. J.; Clarke, A. R. *Biochemistry* **1997**, *36*, 5786−5794.
(59) Katz, J. J.; Crespi, H. L. In *Isotope Effects in Chemical Reactions (ACS Monograph 167)*; Collins, C. J., Bowman, N. S., Eds.; Van Nostrand Reinhold: New York, 1970; p 286−363.
(60) Ogilby, P. R.; Foote, C. S. *J. Am. Chem. Soc.* **1983**, *105*, 3423−3430.
(61) Ermolaev, V. L.; Sveshnikova, E. B. *J. Lumin.* **1979**, *20*, 387−395.
(62) Beeby, A.; Parker, A. W.; Simpson, M. S. C.; Phillips, D. *J. Photochem. Photobiol., B* **1992**, *16*, 73−81.
(63) Nitzan, A. *Chemical Dynamics in Condensed Phases: Relaxation, Transfer, and Reactions in Condensed Molecular Systems*; Oxford University Press: Oxford, 2006.
(64) Klán, P.; Wirz, J. *Photochemisrtry of Organic Compounds*; Wiley: Chichester, 2009.
(65) Siebrand, W. *J. Chem. Phys.* **1967**, *47*, 2411−2422.
(66) Yang, H.; Luo, G.; Karnchanaphanurach, P.; Louie, T.-M.; Rech, I.; Cova, S.; Xun, L.; Xie, X. S. *Science* **2003**, *302*, 262−266.
(67) Liu, X.; Jiang, L.; Li, J.; Wang, L.; Yu, Y.; Zhou, Q.; Lu, X.; Gong, W.; Lu, Y.; Wang, J. *J. Am. Chem. Soc.* **2014**, *136*, 13094−13097.
(68) Pimenta, F. M.; Jensen, R. L.; Holmegaard, L.; Esipova, T. V.; Westberg, M.; Breitenbach, T.; Ogilby, P. R. *J. Phys. Chem. B* **2012**, *116*, 10234−10246.
(69) Jensen, R. L.; Arnbjerg, J.; Ogilby, P. R. *J. Am. Chem. Soc.* **2012**, *134*, 9820−9826.
(70) Lepeshkevich, S. V.; Parkhats, M. V.; Stasheuski, A. S.; Britikov, V. V.; Jarnikova, E. S.; Usanov, S. A.; Dzhagarov, B. M. *J. Phys. Chem. A* **2014**, *118*, 1864−1878.
(71) Scurlock, R. D.; Mártire, D. O.; Ogilby, P. R.; Taylor, V. L.; Clough, R. L. *Macromolecules* **1994**, *27*, 4787−4794.
(72) Marti, C.; Jürgens, O.; Cuenca, O.; Casals, M.; Nonell, S. *J. Photochem. Photobiol., A* **1996**, *97*, 11−18.
(73) Baier, J.; Maisch, T.; Maier, M.; Engel, E.; Landthaler, M.; Bäumler, W. *Biophys. J.* **2006**, *91*, 1452−1459.
(74) Gomes, A.; Fernandes, E.; Lima, J. L. F. C. *J. Biochem. Biophys. Methods* **2005**, *65*, 45−80.
(75) Bilski, P. J.; Karriker, B.; Chignell, C. F. *Chem. Phys. Lett.* **2009**, *475*, 116−119.
(76) Bindokas, V. P.; Jordan, J.; Lee, C. C.; Miller, R. J. *J. Neurosci.* **1996**, *16*, 1324−1336.
(77) To, T.-L.; Fadul, M. J.; Shu, X. *Nat. Comm.* **2014**, *5*, 4072.
(78) Wilkinson, F.; Helman, W. P.; Ross, A. B. *J. Phys. Chem. Ref. Data* **1995**, *24*, 663−1021.
(79) Heelis, P. F.; Parsons, B. J.; Phillips, G. O.; McKellar, J. F. *Photochem. Photobiol.* **1978**, *28*, 169−173.
(80) Lin, J. Y.; Sann, S. B.; Zhou, K.; Nabavi, S.; Proulx, C. D.; Malinow, R.; Jin, Y.; Tsien, R. Y. *Neuron* **2013**, *79*, 241−253.
(81) Ryumina, A. P.; Serebrovskaya, E. O.; Shirmanova, M. V.; Snopova, L. B.; Kuznetsova, M. M.; Turchin, I. V.; Ignatova, N. I.; Klementieva, N. V.; Fradkov, A. F.; Shaklov, B. E.; Zagaynova, E. V.; Lukyanov, K. A.; Lukyanov, S. A. *Biochem. Biophys. Acta* **2013**, *1830*, 5059−5067.

DOI: 10.1021/ja511940j
J. Am. Chem. Soc. 2015, 137, 1632−1642